An Interpretable Machine Learning Model for Deformation of Multi–Walled Carbon Nanotubes

Upendra Yadav , Shashank Pathrudkar , and Susanta Ghosh , and Susanta Ghosh

¹Department of Mechanical Engineering-Engineering Mechanics, Michigan Technological University, MI, USA

²The Center for Data Sciences, Michigan Technological University, MI, USA

We present a novel interpretable machine learning model to predict accurately the complex rippling deformations of Multi-Walled Carbon Nanotubes (MWCNTs) made of millions of atoms. Atomistic-physics-based models are accurate but computationally prohibitive for such large systems. To overcome this bottleneck, we have developed a machine learning model that comprises a novel dimensionality reduction technique and a deep neural network-based learning in the reduced dimension. The proposed nonlinear dimensionality reduction technique extends the functional principal component analysis to satisfy the constraint of deformation. Its novelty lies in designing a function space that satisfies the constraint exactly, which is crucial for efficient dimensionality reduction. Owing to the dimensionality reduction and several other strategies adopted in the present work, learning through deep neural networks is remarkably accurate. The proposed model accurately matches an atomistic-physics-based model while being orders of magnitude faster. It extracts universally dominant patterns of deformation in an unsupervised manner. These patterns are comprehensible and explain how the model predicts, yielding interpretability. The proposed model can form a basis for an exploration of machine learning toward the mechanics of one and two-dimensional materials.

I. INTRODUCTION

Carbon nanotubes have shown remarkable physical, chemical and electronic properties. Moreover, their deformation can be used to control their chemical, and electronic properties, leading to a large number of applications including nanoelectromechanical systems [I+3]. In experiments, multi-walled carbon nanotubes (MWC-NTs) show periodic wavelike deformation patterns called rippling [2]. Walls of MWCNTs are crystalline membranes having very low bending modulus and very high im-plane modulus. Besides, the inter-wall van der Waals interactions keep them separated and guide the deformation [5]. Under loading, the walls bend to minimize their in-plane strain following a near isometric deformation, leading to rippling patterns.

Accurate and efficient simulation tools to predict the complex deformations of large MWCNTs are needed but still elusive. Quantum—mechanical and molecular simulations are accurate but they are computationally prohibitive for large MWCNTs containing millions of atoms. Towards this, Atomistic—Continuum (AC) models have been developed [5+7] by integrating atomistic and continuum frameworks. State—of—the—art AC models are efficient but still require a significant amount of high—performance computing efforts for large MWCNTs, which is the bottleneck for exploration of the physics of these materials.

Machine Learning (ML) methods such as Deep Neural Networks (DNNs) [2], [2] are intensely investigated for accelerating mechanics, physics, and materials research [10-12], however, so far most of the applications are limited to the prediction of low-dimensional properties, such

as material moduli. On the contrary, discretized material deformation requires prediction in a high-dimensional space. Though the continuum deformation is in the ambient space, the discretized data lies in a very high-dimensional space. For instance, large thick MWCNTs require several millions of degrees of freedom to describe its deformation [5, 13].

Deep Learning models can predict low dimensional (e.g. CNN, Autoencoder [14], [15]) or high dimensional outputs (e.g. Encoder-Decoder [16], [17]). However, these Deep Learning models require high dimensional inputs. State—of—the—art DNNs cannot accurately predict high—dimensional targets from a few input features. The objective of the present study is to create an ML model to accurately and efficiently predict high—dimensional discretized deformations of MWCNTs as output from low—dimensional inputs. This necessitates the reduction of dimension of the output.

An additional challenge for the MWCNTs is that the deformed configuration is a non-linear manifold. Thus the reduced-dimension (called *latent space*) of the deformation is non-linear. Commonly used dimensionality reduction techniques [18] such as Principal Component Analysis (PCA) and classical Metric Multidimensional Scaling are inapplicable for the present problem since they are based on linear models. Nonlinear Dimensionality Reduction techniques (also called Manifold Learning) such as Isomap, Locally-Linear Embedding, and Umap are designed to identify the low-dimensional non-linear manifold structure of the data [19], [20]. In these techniques, an approximate low-dimensional neighborhood graph embedded in the high-dimension is obtained following the manifold structure of the data. However, to accurately predict the deformation of MWCNTs we need an accurate, smooth, and functional representation of the mapping from the high-dimensional to a low-

^{*} Address for correspondence: susantag@mtu.edu

dimensional manifold such that it respects the constraints of the deformation. Just visualization or approximate discrete representations of the low-dimensional manifold are not sufficient for the present purpose. Functional Principal Component Analysis (FPCA) 21, 22 provides a smooth functional representation of the data, which is analogous to Kosambi-Karhunen-Loève Expansion [23], [24]. FPCA represents a stochastic process through a linear combination of an infinite number of orthogonal functions. These orthogonal functions are the functional counterparts of principal components in the standard Principal Component Analysis. However, we found that the FPCA cannot respect any geometric constraint of the system since these orthogonal functions need not satisfy any constraint. MWCNTs has periodicity constraint along the circumference due to its cylindrical structure. As a consequence FPCA yields discontinuous and erroneous predictions for MWCNTs, which is demonstrated in the present work (see Sec. IIIA).

In the present work, we propose to extend FPCA by designing a basis set of functions to satisfy this constraint exactly. We call the proposed technique constrained-FPCA (c—FPCA). The proposed c-FPCA technique alleviates the curse of dimensionality by providing lowdimensional functional representations for the deformations of MWCNTs. The proposed semi-supervised ML model includes two steps (i) unsupervised dimensionality reduction (via proposed c-FPCA) of the deformed manifold and (ii) supervised learning (via DNN) of deformation in the reduced dimension. Henceforth, the proposed ML model is referred to as the Deformation Manifold Learning (DML) model, shown in Fig. 1. It takes the details of the MWCNT system and its boundary conditions as inputs and predicts its high-dimensional discretized deformation. The proposed model and the data

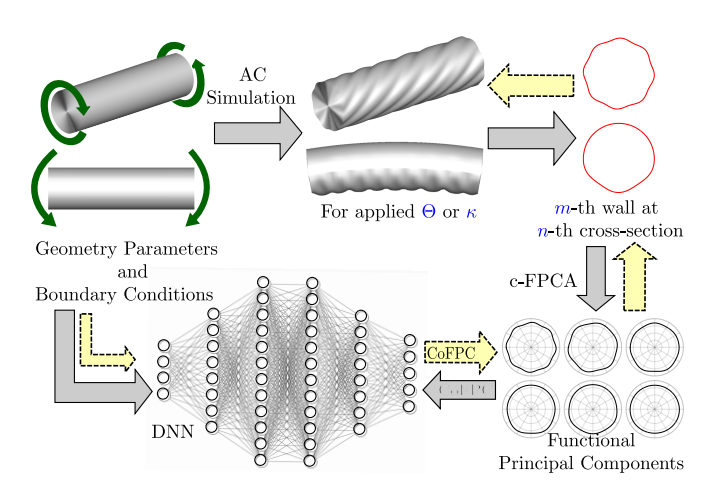


FIG. 1. Schematic of the present framework involving the data generation via AC simulation and the proposed Deformation Manifold Learning(DML) model. The DML model includes: c–FPCA and DNN. Firm arrows show data generation and training, and dashed arrows show prediction via the proposed model.

preparation are described in Sec. II.

Despite their applicability and accuracy, ML models are often criticized as "black—box" or non-comprehensible. Recently there is a surge in efforts to produce intelligible knowledge about the problem through ML models, this ability is referred to as interpretability [25]. The proposed model is interpretable since the *latent space* of deformation is comprehensible through the functions spanning it. The interpretability and accuracy of the model are described in Sec. [III] See Supplemental Material (SM) at [URL] for a list of acronyms and details of the present method.

II. DEFORMATION MANIFOLD LEARNING MODEL

In this section, we describe the deformation data preparation (Sec. $\overline{\text{II A}}$) and the elements of the proposed DML model (Sec. $\overline{\text{II B}}$ and $\overline{\text{II C}}$), whose schematics is given in Fig. $\overline{\text{II}}$. We focus on complex distributed periodic buckling patterns (rippling) of MWCNTs under torsion and bending $\overline{\text{26}}$. An atomistic–continuum model (namely Foliation model $\overline{\text{5}}$) is used to generate the training data for the proposed DML model. See Sec. B of SM at [URL] for more details on the Foliation Model. To represent thick MWCNTs commonly found in the experiments, we are simulating $(5,5), (10,10), \cdots, (5N_w, 5N_w)$ MWCNTs walls, with $N_w = 10$ to $N_w = 40$ in the increment of 5, where N_w is the number of walls. These 7 simulations $(N_w = 10, 15, \cdots, 40)$ are used in training.

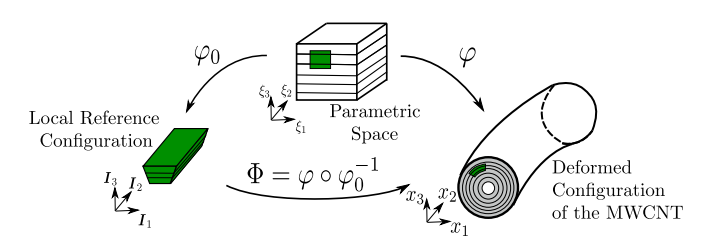


FIG. 2. Illustration of the kinematics showing the configuration spaces, deformation maps, and coordinate axes.

A. Kinematics of MWCNTs and Data Preparation

A configuration map (φ_0) is an injective mapping from parametric space to the local reference configuration. Another map (φ) is from parametric space to Euclidean space, \mathbb{R}^3 as shown in Fig. 2. The deformation map is then defined as $\Phi = \varphi \circ \varphi_0^{-1}$. The energy density of the deformed MWCNT can be computed in terms of the right Cauchy–Green strain field, the curvature tensor field, and the transverse–to–the–wall stretch field of the deformation map (Φ) following the atomistic–continuum model. See Sec. B of SM at [URL] for more details on the atomistic–continuum model.

To learn the deformation pattern of entire MWCNT, multiple sets of simulations would be required. To reduce the number of simulations we decomposed the do-

main into several cross-sections (N_{cs}) at regular intervals along its length. Due to the periodicity of the rippling deformation, this decomposition strategy increases the size of the data set. Let's assume that the ξ_3 coordinate of the m-th tube in the parametric domain is given by ξ_3^m and each tube is discretized along the ξ_2 direction as $\{\xi_2^n\}_{n=1}^{N_{cs}}$. Where N_{cs} denotes the number of cross-sections taken along the tube length. Thus, discretizing the deformed configuration (Φ) along ξ_1 (circumference) and ξ_2 (length) yields a collection of deformed cross–sections, which are parametric curves of ξ_1 , as $\Phi \to \{\Phi_1(\xi_1, \xi_2^n, \xi_3^m), \Phi_2(\xi_1, \xi_2^n, \xi_3^m), \Phi_3(\xi_1, \xi_2^n, \xi_3^m)\},$ $m=1,\cdots,N_w; n=1,\cdots,N_{cs}$. These curves can be further reparametrized in the cylindrical coordinate as $\{\theta(\xi_1), \Phi_2(\theta(\xi_1), \xi_2^n, \xi_3^m), r(\theta(\xi_1), \xi_2^n, \xi_3^m)\}$. Following the decomposition technique, the total deformation of each point (ξ_1, ξ_2, ξ_3) for m-th wall at n-th cross-section of a MWCNT can be represented through two parts, (i) an in–plane radial deformation $r(\theta(\xi_1), \xi_2^n, \xi_3^m)$ in the undeformed cross-sectional plane, and (ii) axial deformation $\Phi_2((\theta(\xi_1), \xi_2^n, \xi_3^m)).$

B. Dimensionality Reduction through Proposed Constrained-FPCA

1. FPCA

The cross–sections of the MWCNTs are given by the mapped (ξ_1, ξ_3) planes for different ξ_2 in the deformed configuration, which constitutes the data set $\{r_i(\theta)\}_{i=1}^N$ of length N. Let us assume the radial deformations of each tube are sampled from a stochastic process $R(\theta)$, $\theta \in \mathcal{T} = (0, 2\pi)$, such that its second derivative is square–integrable. This smoothness of the deformation map is a necessary condition since the energy of a MWCNT is a function of curvature of its walls. We suppose that $R(\theta)$ can take any of the values $r_i(\theta) \in \mathcal{H}^2(\mathcal{T})$, $i = 1, \dots, N$. Where $\mathcal{H}^2(\mathcal{T})$ is Hilbert space. We denote the $L^2(\mathcal{T})$ inner product of functions ϕ_i , $\phi_j \in \mathcal{H}^2(\mathcal{T})$ with $\langle \phi_i, \phi_j \rangle : \int_{\mathcal{T}} \phi_i(\theta) \phi_j(\theta) d\theta$.

Let the mean and the covariance functions of $R(\theta)$ are denoted by $\mu(\theta)$ and $v(\theta, \vartheta) = \text{Cov}(R(\theta), R(\vartheta))$. Invoking the Kosambi–Karhunen–Loève Expansion theorem [23], [24], the centered process can be expressed as

$$R(\theta) - \mu(\theta) = \sum_{k=1}^{\infty} \bar{c}_k \, \psi_k(\theta)$$

Here, $\bar{c}_k = \langle (R(\theta) - \mu(\theta)), \psi(\theta) \rangle$. Where $\psi_k(\theta), k = 1, 2, \cdots$, are the orthonormal eigenfunctions of the following eigenvalue problem $\int_{\mathcal{T}} v(\theta, \vartheta) \, \psi(\theta) d\vartheta = \lambda \, \psi(\theta)$.

These eigenfunctions, $\psi_k(\theta)$, are henceforth referred to as functional principal components (functional–PCs). Assuming a finite set of eigenfunctions is sufficient to approximate the centered stochastic process, $R(\theta) - \mu(\theta)$, its *i*-th sample can be written as

$$r_i(\theta) - \mu(\theta) \approx \sum_{k=1}^{K} \bar{c}_{ik} \, \psi_k(\theta), \ i = 1, \cdots, N$$
 (1)

Interpretation of eigenfunctions: The first eigenfunction ψ_1 represents the principal mode of variation of the data set. The k-th eigenfunction ψ_k is the k-th most dominant mode of variation orthogonal to $\{\psi_i\}_{i=1}^{k-1}$. To solve the aforementioned eigenvalue problem in $\mathcal{H}^2(\mathcal{T})$ we choose a convenient finite-dimensional basis and look for solutions in terms of that predefined basis. However, choosing any arbitrary basis for FPCA will not work, since the deformed configurations of MWCNTs have geometric constraints that need to be satisfied by the eigenfunctions and hence also needs to be satisfied by the basis. Erroneous predictions via FPCA is demonstrated in Sec. III A. To solve the eigenvalue problem while satisfying a constraint can be a difficult task, in the following we reformulate the FPCA in a function space whose every element satisfies the constraint exactly.

2. Proposed Constrained-FPCA

In order to alleviate the above mentioned problem, a basis $\mathcal{B} = \{ \phi_k \in \mathcal{H}^2(\mathcal{T}), g(\phi_k) = 0, k = 1, \cdots, K \}$ is chosen. This basis \mathcal{B} , encodes the geometric constraint (periodic constraint) of the deformation of MWCNTs via the function $q(\phi_k) = 0$, which is crucially important and specializes the FPCA for the systems with any geometric constraint. We call this novel technique constrained-FPCA (c-FPCA). We rewrite the data set, $\{r_i(\theta)\}_{i=1}^N$, the eigenfunction $\psi(\vartheta)$, and the covariance function $v(\vartheta,\theta)$ in terms of the basis \mathcal{B} and solve the aforementioned eigenvalue problem to obtain the functional–PCs. $\psi_k(\vartheta)$. Subsequently, the function $r_i(\theta)$ is represented in terms of functional-PCs using the Eq. 11 and their corresponding coefficients (\bar{c}_{ik}) are referred here as coefficients of functional-PCs (CoFPCs). The i-th sample can be written in terms of the basis, \mathcal{B} , as

$$r_i(\theta) - \mu(\theta) = \sum_{k=1}^{K} c_{ik} \, \phi_k(\theta), \ i = 1, \dots, N$$

$$C_{ik} \in \mathbb{R}$$
(2)

In this work, we have chosen the Fourier Basis for ϕ_k . The eigenfunction's representation in the basis \mathcal{B} as

$$\psi(\theta) = \sum_{k=1}^{K} b_k \phi_k(\theta), \ b_k \in \mathbb{R}$$
 (3a)

$$\psi(\theta) = \phi(\theta)^t \mathbf{b}, \ \mathbf{b} \in \mathbb{R}^K$$
 (3b)

The covariance function can be written in the basis \mathcal{B} as

$$v(\vartheta, \theta) = \frac{1}{N} \phi(\vartheta)^t \mathbf{C}^t \mathbf{C} \phi(\theta)$$
 (4)

the principal component weight functions $\psi_k(s)$ given as

$$\psi_{k} = \underset{\substack{\|\psi\| = 1, \langle \psi, \psi_{f} \rangle = 0 \\ \text{for } i = 1, \dots, k-1}}{\text{arg max}} \operatorname{Var} \left(\int_{\mathcal{T}} (\mathbf{R}(\theta) - \mu(\theta)) \psi(\theta) d\theta \right)$$
 (5)

should satisfy the eigenvalue problem mentioned in the main manuscript. Hence, the eigenvalue problem can be

rewritten as

$$\int_{\mathcal{T}} v(\vartheta, \theta) \psi(\theta) dt = \frac{1}{N} \int_{\mathcal{T}} \phi(\vartheta)^t \mathbf{C}^t \mathbf{C} \phi(\theta) \phi(\theta)^t \mathbf{b} dt$$
$$= \phi(\vartheta)^t N^{-1} \mathbf{C}^t \mathbf{C} \mathbf{W} \mathbf{b} = \lambda \phi(\vartheta)^t \mathbf{b}$$

Where the $K \times K$ symmetric matrix **W** such that $W_{i,j} = \langle \phi_i, \phi_j \rangle$. Defining $\mathbf{u} = \mathbf{W}^{1/2}\mathbf{b}$, the above equation can be expressed as a symmetric eigenvalue problem

$$N^{-1}\mathbf{W}^{1/2}\mathbf{C}^t\mathbf{C}\mathbf{W}^{1/2}\mathbf{u} = \lambda \mathbf{u}$$
 (6)

Which can be solved for the eigenvector \mathbf{u} . The components of each eigenfunction can be found as $\mathbf{b} = \mathbf{W}^{-1/2}\mathbf{u}$. The principal basis can be computed as $\psi(\vartheta) = \phi(\vartheta)^t \mathbf{b}$.

The dimension of the problem is significantly reduced by obtaining a K (number of functional–PCs) much smaller than the size of the discretized $r_i(\theta)$.

C. Learning in the Reduced Dimension through Deep Neural Networks

We have used Deep Neural Networks (DNNs) to map the MWCNT system parameters to its deformation in the reduced dimension. The DNN architecture takes the Geometry parameters and Boundary conditions as input and outputs CoFPCs. The 4 Inputs for the proposed DNN are: Geometry parameters (i) total number of walls in the MWCNT (N_w) , (ii) the wall number $(m, m = 1, \dots, N_w)$, and (iii) the length coordinate $(\Phi_2(\xi_2^n), n=1,\cdots,N_{\rm cs});$ (iv) Boundary Conditions: Angle of twist (Θ) or Curvature (κ) , per unit length. The dimension of the output layer is the number of CoFPCs. which is decided based on the accuracy required (in c-FPCA), details of which are provided in Sec. III B. In supervised learning 8 DNNs are trained using some set of known inputs and outputs before we use them to predict for unknown inputs. DNN (\mathcal{N}) is a composite function of weights $\bar{\mathbf{w}}$ and biases $\boldsymbol{\beta}$ that maps inputs x_i to y_i . The objective is to update these weights \mathbf{w} and biases β to minimize the difference between true output y and predicted output \hat{y} , defined by a cost function $\mathcal{J}(y,\hat{y})$:

$$\min_{\bar{\mathbf{w}}} \quad \mathcal{J}(y, \mathcal{N}(x_i, \bar{\mathbf{w}})) \tag{7}$$

This is done iteratively by using Stochastic Gradient Descent (SGD) and Backpropagation algorithm [27]. Further, this set of trained weights and biases $\bar{\mathbf{w}} = (\mathbf{w}, \boldsymbol{\beta})$ is used to predict unknown output $y_i = \mathcal{N}(x_i, \bar{\mathbf{w}})$ for given input x_i .

DNNs are prone to overfitting and often fail to work accurately for test data. To alleviate the overfitting of the DNN multiple regularization [28], [29] and normalization [30] strategies are adopted in the present work.

The DNN architectures used in our work consist of approximately 40 thousand learning parameters and uses mean squared error of CoFPCs as the loss function (see Sec. C of SM at [URL] for more details on the DNN architecture). Three DNNs are trained for predicting the

following deformations of MWCNTs: (i) In–plane deformation under torsion, (ii) in–plane, and (ii) out–of–plane (axial) deformation under bending. Unlike torsion, in bending the axial deformation is not negligible, hence we have used two DNNs for in–plane and axial deformations.

III. Results

A. Limitations of FPCA

In this subsection, we show that the failure of FPCA to satisfy the constraint exactly leads to inaccurate dimension reduction and hence inaccurate prediction of the deformation via the DML model. To show this limitation of FPCA two approaches are taken here:

- (i) FPCA coupled with DNNs
- (ii) FPCA coupled with constrained–DNNs.

These approaches were used to predict the deformation of twisted MWCNTs. In the first approach, we use DNN on the reduced dimension, which is obtained via FPCA. We found that it yields discontinuity in the deformation due to the violation of constraints by the FPCA as shown in Fig. \Box a,b. To overcome the discontinuity, in the second approach we have enforced the constraint through the DNN by modifying its objective function:

$$\tilde{\mathcal{J}}(y, \mathcal{N}(x_i, \bar{\mathbf{w}})) = \mathcal{J}(y, \mathcal{N}(x_i, \bar{\mathbf{w}})) + \lambda \mathcal{E}_P$$
 (8)

where \mathcal{E}_P is the error due to the violation of the constraint. The unknown parameter λ decides the degree of enforcement of the constraint. The penalty parameter, λ , provides a balance between the two errors. The optimum λ is obtained here by using the L-curve method [31]. See Sec. D of SM at [URL] for further details on the L-curve. Even for the optimum λ , the constraint-DNNs can satisfy the constraint only approximately (not exactly). While the constraint-DNN could reduce the discontinuity, it significantly compromises accuracy everywhere else as shown in Fig. [3c, d. For the rest of this paper, we focus on the proposed c—FPCA method to predict the deformation, which is designed to satisfy the constraint exactly.

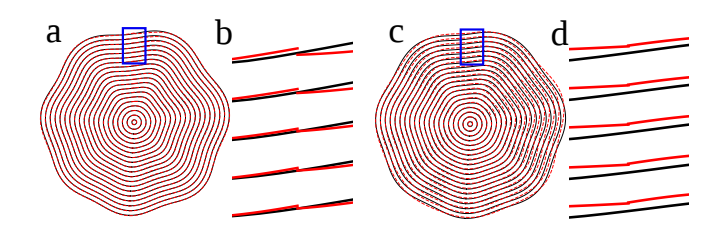


FIG. 3. Cross—sections of MWCNT obtained using two approaches of DML model (---) that uses FPCA: (a) FPCA coupled with DNN and (c) FPCA coupled with the constrained—DNN. These two approaches are compared against the AC model (—). (b) and (d) are the close—up views of the blue boxes corresponding to (a) and (c). (b) Shows a discontinuity in the DML model and (d) shows increases error in prediction everywhere.

B. Dimensionality Reduction via the Proposed Constrained FPCA

The proposed c-FPCA dimensionality reduction could capture 99% variability of the deformation data set through only 14 and 4 functional-PCs for torsion and bending respectively, as shown in Fig. 4. To capture 99.9% variability, the corresponding numbers are 16 and 6 respectively. The associated (16 and 6) CoFPCs are used as the outputs of DNNs. To obtain the functional— PCs we started with 64 basis functions to represent data vectors of size up to several hundred. This demonstrates up to two orders of magnitude dimensionality reduction via the present approach. Owing to the high accuracy of c-FPCA, DNNs need to learn in significantly reduced dimensions, yielding higher accuracy. Further, c-FPCA returns only a few dominant modes having a perspicuous pattern, which makes it easier for DNN to learn (see Fig. 5 and 6 of SM at [URL]).

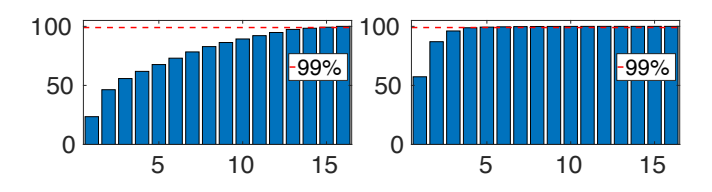


FIG. 4. Cumulative % variance captured by principal components for MWCNTs under torsion (left) and bending (right).

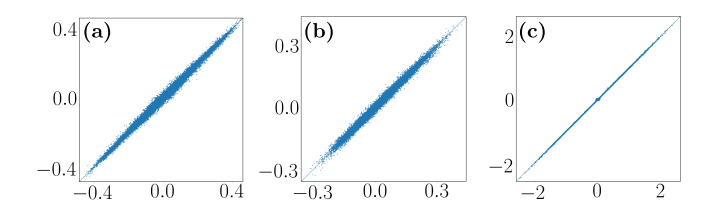


FIG. 5. Correlation plots for test set CoFPCS of (a) in–plane deformation in torsion, (b) in–plane and (c) out–of–plane deformation in bending. R = 0.9943(a), 0.9931(b), 0.9991(c).

C. Accuracy

While predicting through the DML model, for a given MWCNT system and loading, at first, the DNN predicts the CoFPCs, which lie in the low-dimensional latent space. Subsequently, the high-dimensional deformed cross-sections containing all the walls (Fig. 6 (bottom) and Figs. 7 e, f, g) is obtained through inverse c-FPCA. Further, these deformed cross-sections are concatenated through the length coordinate to generate the 3D deformed shape. Since the functional-PCs are non-zero almost everywhere, it is imperative that we predict CoFPCs very accurately. To achieve very high accuracy for DNNs we have adopted the following strategies: (i) regularization techniques, (ii) hyper-parameter tuning, and (iii) features-normalization, (see Sec. IIC).

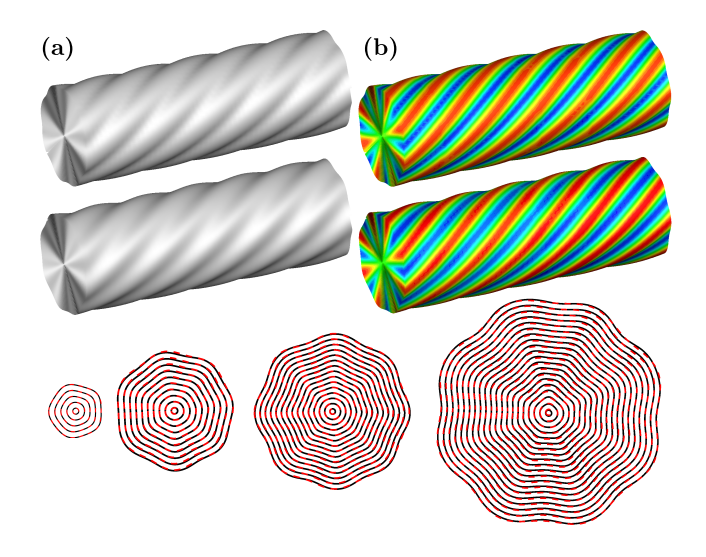


FIG. 6. (a) Twisted 40 walled CNT obtained via AC (top) and DML (bottom) model. (b) Radial deformation colormap (Red: high, Blue: low). Alternate walls of cross–sections obtained via AC (——) and DML (---) models, for 10, 20, 30, and 40 walled CNTs.

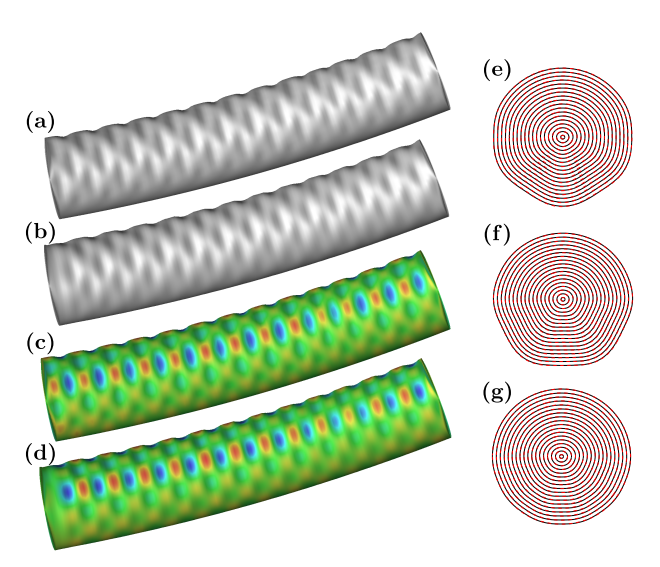


FIG. 7. Bent 35-walled CNT obtained via AC (a,c) and DML (b,d) model.(c) and (d) show colormap of radial deformations corresponding to (a) and (b). (e-g) Alternate walls of cross-sections obtained via AC (——) and DML (——) model.

The high accuracy of the DNNs is demonstrated through very low relative—mean squared error (order of 10^{-4}) for the validation data and excellent correlations (R>0.993) for the test data as shown in Fig. 5.

Predictions by the proposed DML model is compared against the AC model for two types of systems: (i) known systems but unknown loading, (ii) unknown systems and unknown loading, Deformation morphologies under torsion and bending obtained through AC and DML models are provided for the known and unknown

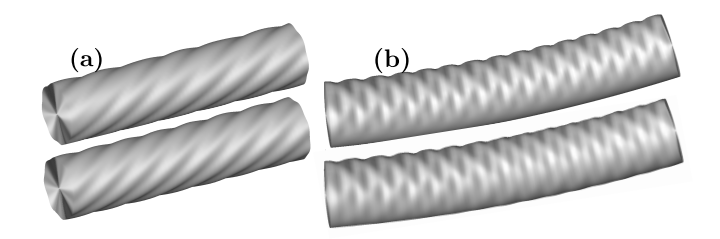


FIG. 8. Comparison of AC (top) and DML (bottom) models for a 32 walled CNT (system which is not a part of training data) under torsion (a) and bending (b).

systems in Fig. (6.7) and in Fig. 8 respectively. The proposed DML model matches remarkably well with the AC model for unknown loading as evident from the deformed surfaces and cross—sections. Their match is quite accurate even when both the system and the loading are unknown (as long as the unknown system is within the range of the training data). This obviates the need for AC simulations for such systems, yielding huge computational savings. However, if an MWCNT lies way outside the range of the training data its accuracy might go down since it might exhibit a deformation pattern that doesn't occur in the training.

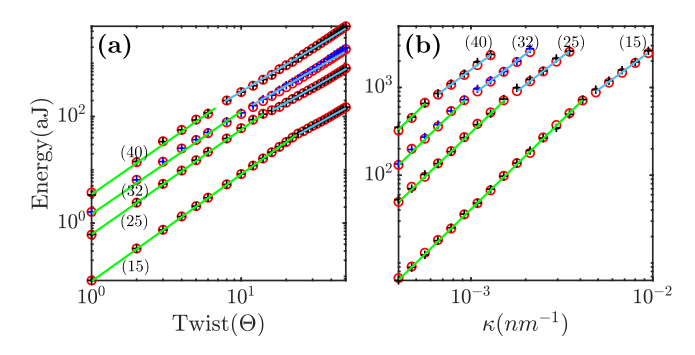


FIG. 9. Energy comparison for (15, 25, 32, 40 –walled) MWC-NTs under torsion (a) and bending (b) via AC (o) and DML model (+). 32 walled CNT (+) is an unknown system. The lines (—) and (—) are drawn to highlight pre– and post–buckling regimes.

To quantify the accuracy, we compute the relative error in the predicted deformed configurations. The maximum relative error is found to be $\approx 1\%$ for the 32–walled CNT, which is an unknown system under unknown loading. See Sec. F of SM at [URL] for the details on the quantification of accuracy.

We attribute the high accuracy of the proposed model to the accuracy in both the dimensionality reduction and learning through DNNs. The deformation obtained from CoFPCs (output of the DML model) is used to compute the energy via a discretization. See Sec. F of SM at [URL] for the details of energy calculation. The energy computed through the DML and the AC model matches very well for both known and unknown systems, as shown in Fig. [9].

The proposed model is significantly more efficient than the AC model. The AC model requires tens or hundreds of *total CPU* hours in parallel processing to simulate each of the MWCNTs. Whereas, inference via the proposed model (upon training), requires only about ten seconds for an unknown MWCNT.

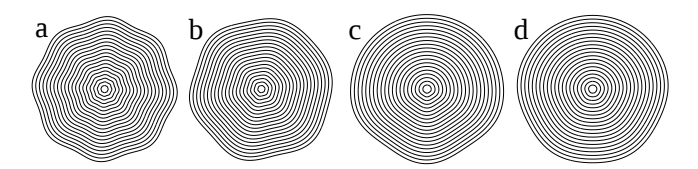


FIG. 10. Functional principal components of MWCNTs under torsion (a,b) and bending (c,d).

D. Interpretability of the model

Recently several efforts have been made to overcome the "black box" nature of ML models and to make them more comprehensible to humans, through formulating interpretation techniques [25]. Herein, we explore the model-based-interpretability (as defined in [25]) of the proposed model. The proposed model can extract dominant (principal) modes of deformed configurations and their relative contribution in an unsupervised manner. A few principal components of the deformation of MWC-NTs under torsion and bending are shown in Fig. [10]. See Sec. E of SM at [URL] for additional principal components. The rippling deformation of MWCNTs under torsion follows a sequence of ridge and furrows, whereas, in case of bending it resembles the diamond buckling pattern [13]. These key patterns of deformation are captured through the functional principal components (Fig. 10). So far these key deformed patterns were approximately identified manually for individual MWCNTs. The principal components of deformation automatically identified in the present model show qualitative similarity with those identified manually in [7, 26, 32]. These functional-PCs are universal since they are obtained from the entire data set. This fact enhances the model's predictive capability on unseen systems and hence explains the generalizability (performance for unseen systems) of the model. The DNNs learn the reduced dimension spanned by the functional–PCs. The principal modes of deformations are easy to comprehend thus enhance the understanding of how the proposed model works, which makes it an interpretable model.

IV. Conclusion and Discussions

In this study, a novel interpretable machine learning model is proposed, which predicts high–dimensional deformed configurations of MWCNTs accurately and efficiently using only 4 inputs. It combines an unsupervised dimensionality reduction of the deformed configuration space and a supervised learning in the reduced space.

To conclude this study, we summarize its main fea-

tures. Firstly, a novel dimensionality reduction technique is proposed that extends FPCA to respect the constraints of deformation exactly. This improves accuracy in low–dimensional representation of deformation and enables accurate prediction of high–dimensional deformation of MWCNTs. Secondly, the proposed model is remarkably accurate for unknown systems and unknown loading. This capability eliminates expensive AC simulations for systems beyond what is used in the training, yielding a massive gain in computational efficiency. Thirdly, the principal components are comprehensible and thus help to elucidate how the model predicts high–dimensional deformation through learning the space of functional–PCs,

leading to model–interpretability.

The proposed model will serve as a basis for the exploration of machine learning for nanotubes and 2D materials.

Acknowledgments: The work is supported by NSF (CMMI MoMS) under grant number 1937983. We acknowledge Superior, a high-performance computing facility at MTU. This work used the Extreme Science and Engineering Discovery Environment (XSEDE), which is supported by the NSF grant number ACI-1548562. This work used the XSEDE Bridges at the Pittsburgh Supercomputing Center through allocation MSS200004.

- P. Williams, S. Papadakis, A. Patel, M. Falvo, S. Washburn, and R. Superfine, Phys. Rev. Lett. 89, 255502 (2002).
- [2] S. J. Papadakis, A. R. Hall, P. A. Williams, L. Vicci, M. R. Falvo, R. Superfine, and S. Washburn, Phys. Rev. Lett. 93, 146101 (2004).
- [3] M. F. L. De Volder, S. H. Tawfick, R. H. Baughman, and A. J. Hart, Science 339, 535 (2013).
- [4] P. Poncharal, Z. L. Wang, D. Ugarte, and W. A. de Heer, Science 283, 1513 (1999).
- [5] S. Ghosh and M. Arroyo, J. Mech. Phys. Solids 61, 235 (2013).
- [6] M. Arroyo and T. Belytschko, J. Mech. Phys. Solids 50, 1941 (2002).
- [7] M. Arroyo and T. Belytschko, International Journal for Numerical Methods in Engineering 59, 419 (2004).
- [8] Y. Lecun, Y. Bengio, and G. Hinton, Nature 521, 436 (2015).
- [9] K. Hornik, M. Stinchcombe, and H. White, Neural Networks 2, 359 (1989).
- [10] T. Xie and J. C. Grossman, Phys. Rev. Lett. 120, 145301 (2018).
- [11] R. Iten, T. Metger, H. Wilming, L. del Rio, and R. Renner, Phys. Rev. Lett. 124, 010508 (2020).
- [12] L. Lu, M. Dao, P. Kumar, U. Ramamurty, G. E. Karniadakis, and S. Suresh, Proc. Natl. Acad. Sci. U.S.A. 117, 7052 (2020).
- [13] I. Arias and M. Arroyo, Phys. Rev. Lett. **100** (2008).
- [14] P. Z. Hanakata, E. D. Cubuk, D. K. Campbell, and H. S. Park, Phys. Rev. Lett. 121, 255304 (2018).
- [15] P. Z. Hanakata, E. D. Cubuk, D. K. Campbell, and H. S. Park, arXiv preprint arXiv:2008.05298 (2020).
- [16] R. Gómez-Bombarelli, J. N. Wei, D. Duvenaud, J. M. Hernández-Lobato, B. Sánchez-Lengeling, D. Sheberla, J. Aguilera-Iparraguirre, T. D. Hirzel, R. P. Adams, and A. Aspuru-Guzik, ACS central science 4, 268 (2018).
- [17] A. Balu, S. Nallagonda, F. Xu, A. Krishnamurthy, M.-C.

- Hsu, and S. Sarkar, Scientific reports 9, 1 (2019).
- [18] L. Van Der Maaten, E. Postma, and J. Van den Herik, Dimensionality reduction: a comparative review, J Mach Learn Res 10, 66 (2009).
- [19] J. A. Lee and M. Verleysen, Nonlinear Dimensionality Reduction, 1st ed. (Springer, 2007).
- [20] L. McInnes, J. Healy, and J. Melville, arXiv preprint arXiv:1802.03426 (2018).
- [21] F. Yao, H.-G. Müller, and J.-L. Wang, Annals of Statistics 33, 2873 (2005).
- [22] J. Ramsay and B. Silverman, Functional Data Analysis (Springer, 2005).
- [23] H. Stark and J. W. Woods, eds., Probability, Random Processes, and Estimation Theory for Engineers (Prentice-Hall, Inc., USA, 1986).
- [24] P. Jorgensen and M. Song, J. of Mathematical Physics 48, 103503 (2007).
- [25] J. Murdoch, C. Singh, K. Kumbier, R. Abbasi-Asl, and B. Yu, Proc. Natl. Acad. Sci. U.S.A. 116, 22071 (2019).
- [26] M. Arroyo and T. Belytschko, Phys. Rev. Lett. 91, 215505 (2003).
- [27] Y. LeCun, D. Touresky, G. Hinton, and T. Sejnowski, A theoretical framework for back-propagation, in *Proceedings of the 1988 connectionist models summer school*, Vol. 1 (CMU, Pittsburgh, Pa: Morgan Kaufmann, 1988) pp. 21–28.
- [28] L. Prechelt, Early stopping but when?, in Neural Networks: Tricks of the Trade: Second Edition (Springer, 2012) pp. 53–67.
- [29] H. Zou and T. Hastie, Journal of the royal statistical society: series B (statistical methodology) **67**, 301 (2005).
- [30] T. Jayalakshmi and A. Santhakumaran, Int. J. of Computer Theory and Engineering 3, 1793 (2011).
- [31] P. C. Hansen, Analysis of discrete ill-posed problems by means of the l-curve, SIAM Review 34, 561 (1992), https://doi.org/10.1137/1034115.
- [32] J. Zou, X. Huang, M. Arroyo, and S. Zhang, Journal of applied physics 105, 033516 (2009).